PHYSICS OF PLASMAS **17**, 042309 (2010)

Nonlinear simulation of toroidal Alfvén eigenmode with source and sink

Jianying Lang,[1] Guo-Yong Fu,[1] and Yang Chen[2]
[1]*Princeton Plasma Physics Laboratory, Princeton, New Jersey 08543, USA*
[2]*University of Colorado at Boulder, Boulder, Colorado 80309, USA*

(Received 3 January 2010; accepted 24 March 2010; published online 29 April 2010)

Kinetic/magnetohydrodynamic hybrid simulations are carried out to investigate the nonlinear dynamics of energetic particle-driven toroidal Alfvén eigenmode with collision and source/sink. For cases well above marginal stability, the mode saturation is approximately steady state with finite collision frequency. The calculated scaling of saturation level with collision frequency agrees well with analytic theory. For cases near-marginal stability at low collision rates, the mode saturation exhibits pulsation behavior with frequency chirps up and down. © *2010 American Institute of Physics*. [doi:10.1063/1.3394702]

I. INTRODUCTION

In burning plasmas of fusion reactors such as ITER,[1] the fusion product alpha particles can constitute a substantial fraction of the total plasma pressure. These super-Alfvénic energetic particles can drive Alfvén instabilities by tapping the free energy associated with radial gradient of the distribution via wave particle resonances. The driven Alfvén instabilities can in turn cause energetic particle loss to the reactor wall and induce wall damage. Thus it is very important to investigate the nonlinear saturation of Alfvén instabilities and the energetic particle transport.

One of the main candidates causing the anomalous transport of energetic particles is toroidicity-induced Alfvén eigenmode (TAE).[2] TAEs are discrete shear Alfvén eigenmodes with global structure. They can be driven unstable by the spatial gradient of the energetic particle distribution via inverse Landau damping process.[3,4] It is essential to investigate the nonlinear dynamics of TAE to improve the energetic particle confinement. Here, we perform self-consistent nonlinear kinetic/MHD hybrid simulations to study the nonlinear evolution of TAEs using the M3D code.[5] M3D is a three dimensional nonlinear extended-MHD code with multiple level of physics. The code has been successfully applied to study a variety of MHD instabilities in tokamaks and stellarators.[6–12]

In this work, the kinetic/magnetohydrodynamic (MHD) hybrid model of M3D is used. In the model, the thermal plasmas are treated as single fluid and the energetic particles are described using the drift-kinetic equation. The effects of energetic particles enter in the model in the momentum equation via the stress tensor term. The code uses general equilibria with finite beta, finite aspect ratio, and arbitrary plasma shape. Recently, we have added into the code the effects of energetic particle collision with thermal ions and electrons using a simple collision operator. The operator describes the pitch angle scattering as well as particle drag (or slowing down). We also implemented source and sink for energetic particles from neutral beam injection or birth of fusion alpha particles.

In this work, we investigate numerically the effects of energetic particle collision and source/sink on nonlinear dynamics of energetic particle-driven TAE modes. In the collisionless limit, it is well known that the TAEs can saturate nonlinearly due to the flattening of particle distribution function (caused by trapping of resonant particles in the finite amplitude waves). With finite damping due to thermal ions and electrons, the TAEs then decay to zero after saturation. However, particle collision can scatter particles in and out of resonances. This collisional process tends to restore the equilibrium gradient of the particle distribution. The balance of finite nonlinear mode drive with collision and the background damping establishes a steady state nonlinear saturation. These physics processes had been studied analytically in a series of seminal papers of Berk and Breizman.[13–16] It was shown that the mode saturation level scales with collision frequency as $A_{\text{saturation}} \sim \nu^{2/3}$ for pure scattering case or pure slowing down case, where ν is the collision frequency.[16] In their subsequent studies, it was shown that for near-marginal stability cases, the steady state saturation changes into pulsation (or bursting) and explosive phase as collision frequency is reduced to below a critical value.[17] Correspondingly, the mode frequency chirps up and down due to formation and movement of hole and clump in phase space.[18] Our numerical results are consistent with these previous analytical and numerical results in both the steady state saturation regime and the pulsation regime.

Most of previous nonlinear simulation studies of energetic particle-driven Alfvén instabilities neglected the effects of collision and source/sink on nonlinear evolution.[19–22,9,23–26] In few works where the effects of collision and source/sink were considered, simple reduced models such as fixed mode structure were used.[27–31] A self-consistent Fokker–Planck-MHD simulation including slowing down, source/sink and evolving mode structure was also reported.[32] In this work, we have investigated the effects of collision and source/sink systematically using a drift-kinetic/MHD hybrid model in a self-consistent way. In particular, we include self-consistent evolution of eigenmode structure and include both pitch angle scattering and slowing down due to collision. Our numerical simulation results agree with the analytic $\nu^{2/3}$ scaling for the steady sate saturation cases far from marginal stability. Furthermore, we show that the nonlinear saturation exhibits bursting behavior for cases near-marginal stability at low collision rates, consistent with previous simulation results obtained for the bump-on-tail problem.[17]

The outline of this paper is as follows. In Sec. II, we briefly describe the numerical implementation of the particle source and sink. In Sec. III, we present the simulations results in different parameter regimes, including pitch angle scattering dominated regime, slowing down dominated regime, and near-marginal regime. The parameter scaling is compared to the analytical prediction and shows good agreement. The variation in the resonance structure during the nonlinear saturation is also examined. In Sec. IV, we show the convergence study with respect to the particle number and the time step. In Sec. V, summary is given.

II. NUMERICAL MODELS AND BASIC PARAMETERS

This simulation is performed using M3D-K code, which is a hybrid code with thermal plasmas being described as MHD and energetic particles being described drift kinetically. Particle-in-cell δf method is employed in the drift-kinetic simulation of energetic particles. The total distribution function is separated into two parts $f=f_0+\delta f$, f_0 is the equilibrium distribution function, and δf is the perturbed part. In simulations, the perturbed distribution function δf is represented by particle weight $w=\delta f/g$, where g is the particle loading function. The weight evolution equations are listed as Eqs. (B1)–(B7) in Ref. 9. The energetic particle pressure is calculated from the total particle distribution function. More details about the code can be found in Ref. 9.

A. Numerical implementation of source and sink

In this work, we have added the energetic particle collision with thermal ions and electrons into the M3D-K code. We have also added source and sink for energetic particles. In particular, we have implemented the following simple collision operator for energetic particles in the code:

$$C(f) = \nu_d \frac{\partial}{\partial \lambda}(1-\lambda^2)\frac{\partial}{\partial \lambda} f + \frac{\nu}{v^2}\frac{\partial}{\partial v}(v^3+v_c^3)f, \tag{1}$$

where $\lambda=v_\parallel/v$ is the pitch angle, ν is the drag rate (the inverse of slowing down time), and ν_d is pitch angle scattering rate which is related to ν by $\nu_d=\nu v_c^3/2(c^3+v^3)$. Here, v_c is the critical velocity given by

$$v_c^3 = \frac{3\sqrt{\pi}}{4}\frac{m_e}{m_i}\left(\frac{2T_e}{m_e}\right)^{3/2}, \tag{2}$$

and $c=0.17v_0$ is a small artificial constant used to avoid numerical problems when particle speed becomes small. The first term of right hand side of Eq. (1) represents the pitch angle scattering due to collision of energetic ions with thermal electrons and the second term represents slowing down due to collision of energetic ions with thermal ions and thermal electrons.

In simulations, we employ the fourth-order Runge–Kutta method to advance particle trajectory according to the drift-kinetic equation. The pitch angle scattering is modeled using a Monte Carlo method. Thus, the pitch angle is updated at the end of each time step according to the following equation:[33]

$$\lambda_{\text{new}} = \lambda_{\text{old}}(1-2\nu_d\Delta t) \pm \sqrt{(1-\lambda_{\text{old}}^2)2\nu_d\Delta t}, \tag{3}$$

where Δt denotes the time step and the sign $\pm$ is given by a numerical random number generator.

For particle slowing down, the energetic particle speed is updated using the following equation:

$$\frac{dv}{dt} = -\nu\left(v+\frac{v_c^3}{v^2}\right). \tag{4}$$

The simulation particles are initially loaded according to an isotropic slowing down distribution function which is given by

$$g = \frac{1}{v^3+v_c^3}H(v-v_{\max}). \tag{5}$$

The source and sink are implemented through particle injection and particle removal. When simulation particles' speed is smaller than a threshold value, $v<v_{\text{cut}}$, these particles are removed and reinjected back into the plasma uniformly in real space with a fixed speed $v=v_{\max}$ and a random pitch angle. This way of particle recycling preserves the number of simulation particles and maintains the loading distribution function roughly constant in time.

The equilibrium energetic particle distribution is chosen to be

$$f_0 = \frac{n_0}{2(v^3+v_c^3)}\left[1+\text{erf}\left(\frac{v_0-v}{0.2v_A}\right)\right]\exp(-\bar{\psi}), \tag{6}$$

where erf is the error function, $\bar{\psi}=P_\phi/e\Delta\psi$, $P_\phi=e\psi+mv_\parallel RB_\phi/B$ is the toroidal angular momentum, ψ denotes the poloidal flux with $\psi=\psi_{\min}$ at the magnetic axis and $\psi=\psi_{\max}=0$ at the plasma edge, $\Delta\psi=0.37(\psi_{\max}-\psi_{\min})$, and v_0 is the injection speed for beam ions. In the simulations, we choose $v_0=1.7v_A$, $v_{\text{cut}}=0.1v_A$, and $v_{\max}=1.5v_0$, where v_A is the Alfvén speed. Note that the energetic particle distribution decays exponentially for $v>v_0$, the selected value of $v_{\max}$ is sufficiently large for the simulation particles to cover the energetic particle distribution.

B. Basic parameters

For simplicity, the simulation results reported below are based on a zero beta tokamak equilibrium with circular flux surface. The aspect ratio is $R/a=3$. The plasma density profile is uniform. The safety factor profile is $q=1.1+\psi$, where ψ is the magnetic flux surface. Moreover the safety factor at the center is $q(0)=1.1$ and at the edge is $q(a)=2.1$. The maximum energetic particle gyroradius is $\rho_h/a=0.085$. The number of particles and the time step used in our simulations runs to be described below are 4.2×10^6 and $\omega_A\Delta t=0.035$, respectively (unless otherwise specified), with $\omega_A=v_A/R_0$ being the Alfvén frequency. Using this set of parameters and profiles, we obtain the base line case of a single n=1 TAE mode. The contour plot of U of the n=1 mode in a poloidal cross section is shown in Fig. 1. Here U is the stream func-

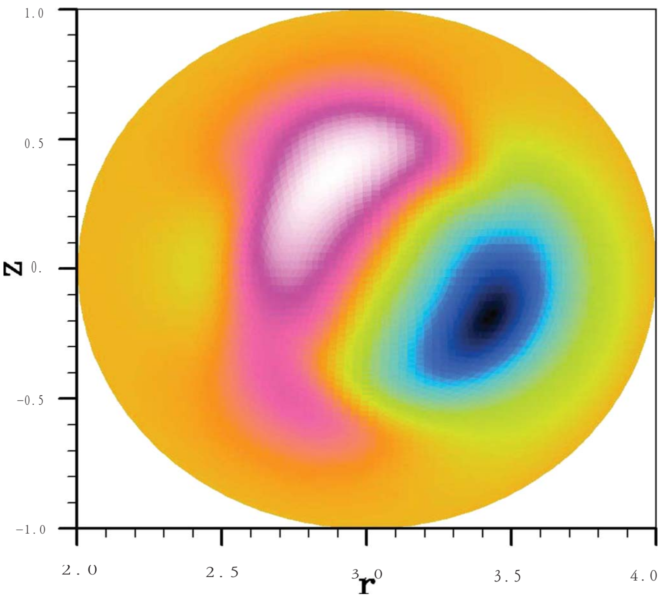

FIG. 1. (Color online) The contour plot of U for the baseline case.

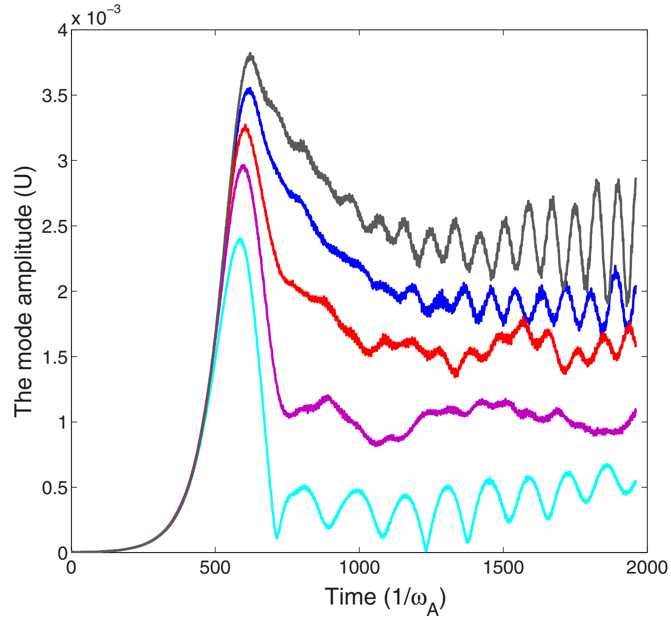

FIG. 2. (Color online) The time evolution of the mode amplitude with only pitch angle scattering at different collision rates. From the top to the bottom, the collision rates are $\nu=1.0\times10^{-3}\omega_A$, $\nu=7.5\times10^{-4}\omega_A$, $\nu=5.0\times10^{-4}\omega_A$, $\nu=2.5\times10^{-4}\omega_A$, and $\nu=5\times10^{-5}\omega_A$.

tion of the incompressional part of the perturbed plasma velocity. The mode frequency and the net growth rate are $\omega/\omega_A=0.32$ and $\gamma/\omega_A=1.3\%$, respectively. The following study is based on this n=1 single TAE mode.

In this paper, we only take into account the linear MHD response of thermal plasmas for simplicity but include both the linear and nonlinear effects for energetic particles. In particular, we focus on the effects of collision and source/sink on nonlinear saturation of energetic particle-driven Alfvén modes.

III. SIMULATION RESULTS OF NONLINEAR SATURATION OF SINGLE TAE

In this section, we systematically study the effect of pitch angle scattering and slowing down with source/sink on the nonlinear saturation of n=1 TAE in various parameter regimes.

A. Effect of pitch angle scattering on nonlinear saturation

First we investigate the effect of pitch angle scattering on nonlinear saturation of the n=1 TAE mode for the baseline case. The slowing down effect is turned off. Physically, the TAE mode saturates due to flattening of particle distribution function in the resonance region. This flattening is caused by the fast bounce motion of the resonant particles trapped in the finite amplitude wave. However, pitch angle scattering can scatter particles out of resonance region (also into the resonance region) and thus can restore the gradient of particle distribution. The balance of these two competing effects establishes a steady state mode saturation with background mode dissipation. The saturation level in the presence of pitch angle scattering can be estimated by a simple model $\omega_b \approx \nu_{\rm eff}\gamma_L/\gamma_d$,[16] where ω_b is the bouncing frequency of trapped resonant particles, γ_L is the linear energetic particle drive, γ_d is the damping rate caused by the background dissipation, and $\nu_{\rm eff}\approx\nu_d(\omega/\omega_b)^2$ is the effective pitch angle scattering rate. Here, ω is the mode frequency. Since the bouncing frequency ω_b is proportional to the squared root of the mode amplitude, the mode saturation amplitude scales as $\nu_d^{2/3}$.

We now present our numerical results of nonlinear mode saturation with pitch angle scattering only. Figure 2 shows the time evolution of the mode amplitude of the stream function U for various pitch angle scattering rates. In simulations, the scattering rate is specified by the slowing down rate using $\nu_d=\nu v_c^3/2(c^3+v^3)$ $(c=0.17v_0)$. We vary the scattering rate by setting different slowing down rates as a single collision parameter although slowing down process is not considered in this case. Note also we have added a small artificial term c^3 in the denominator so that the scattering rate is kept finite at small velocity. In this pitch angle scattering scan, other parameters are all fixed. From Fig. 2, it is apparent that there is little difference in the linear regime for different scattering rates but the nonlinear saturation level increases with ν monotonically. Furthermore, we can also observe that there are small fast oscillations associated with the nonlinear saturation. These fast oscillations are probably related to the bouncing motion of resonant particles trapped in the TAE waves. Further detail of these oscillations will be discussed below.

Figure 3 shows the corresponding scaling between the saturation level of the mode amplitude and the scattering rate. In this plot, the value of the saturation amplitude is obtained by averaging over the fast oscillations in the quasi-steady phase for each scattering rate. The linear regression power fitting of the simulation data gives the scaling of $U\simeq0.21\nu^{0.65\pm0.13}$, where the numerical coefficient is normalized according to the code unit. Compared to the analytical scaling of $U\sim\nu_d^{2/3}$ shown in Ref. 14, where

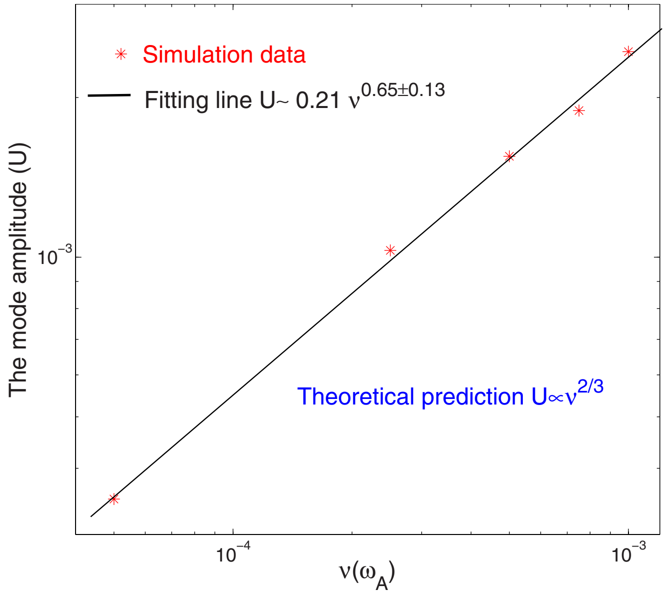

FIG. 3. (Color online) The nonlinear saturation level of the mode amplitude as a function of collision rate in the presence of pitch angle scattering only.

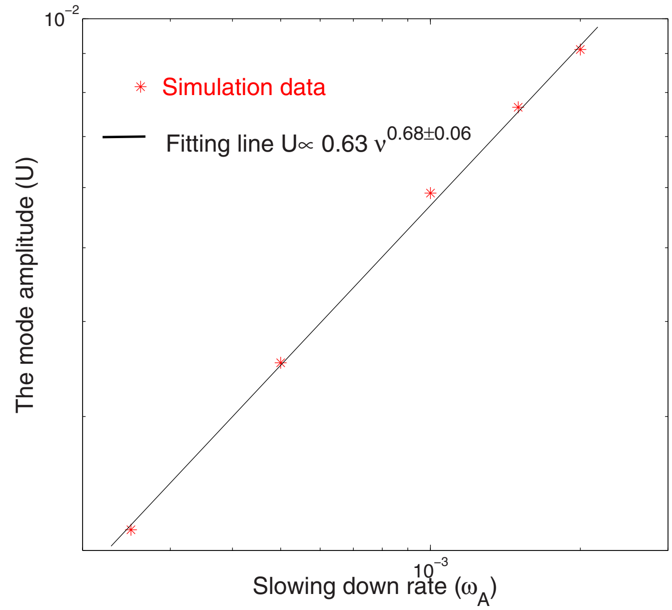

FIG. 5. (Color online) The nonlinear saturation level of the mode amplitude as a function of collision rate in the presence of slowing down only.

$\nu_d = \nu v_c^3/2(c^3+v^3)$ $(c=0.17v_0)$, simulation results agree very well with the analytical prediction on the power scaling.

B. Effect of slowing down on mode nonlinear saturation

Next we investigate the nonlinear saturation with particle slowing down, particle source, and sink. The pitch angle scattering is turned off. Although the effective collision rate induced by pitch angle scattering and slowing process is totally different, the scaling between the nonlinear saturation level versus the diffusion rate ν_d and the slowing down rate ν is the same according to the analytical calculation shown in Ref. 14. That is, $U \sim \nu^{2/3}$. The drag rate (slowing down rate) considered here ranges from $\nu = 2.5\times10^{-4}\omega_A$ to $\nu = 2.0\times10^{-3}\omega_A$. In Fig. 4, we show the time evolution of the mode amplitude at different slowing down rates. We observe that the mode saturates in quasisteady state. The linear regression power fit of the data for nonlinear saturation level versus slowing down rate gives $U \simeq 0.63\nu^{0.68\pm0.06}$, as shown in Fig. 5.

Just like the case of pure pitch angle scattering, there is a little difference in the linear regime for different slowing down rates and similar quasisteady states are obtained in the

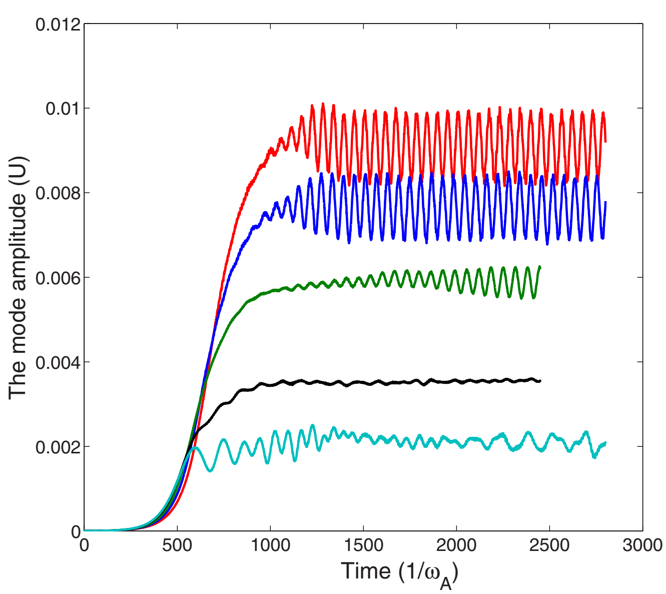

FIG. 4. (Color online) The time evolution of the mode amplitude with only slowing down process at different slowing down rates. From top to bottom, the slowing down rates are $\nu=2.0\times10^{-3}\omega_A$, $\nu=1.0\times10^{-3}\omega_A$, $\nu=5.0\times10^{-4}\omega_A$, and $\nu=2.5\times10^{-4}\omega_A$.

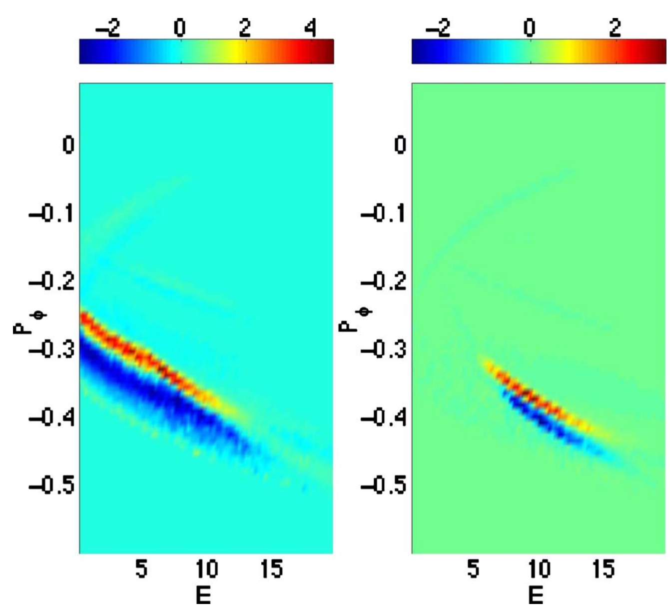

FIG. 6. (Color online) The contour plots of the δf as a function of toroidal angular momentum and energy for fixed $\Lambda=\mu B/E=0.25$. The right plot is for collisionless condition and the left plot is for slowing down only with slowing down rate $\nu=5.0\times10^{-4}\omega_A$.

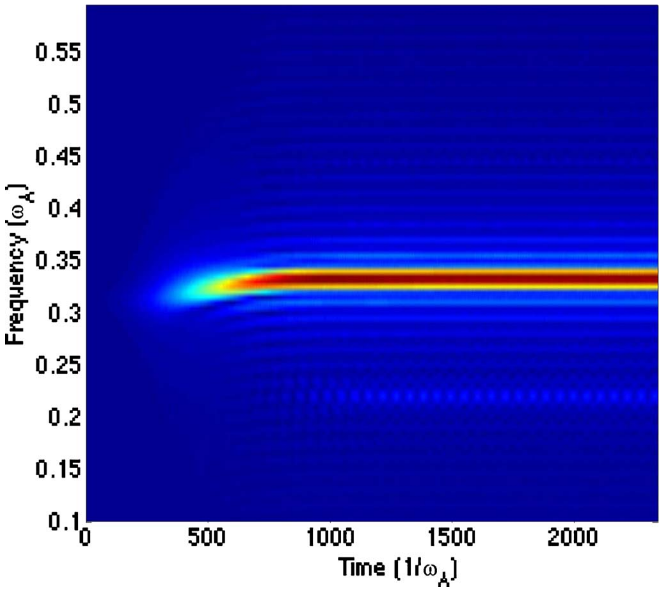

FIG. 7. (Color online) The contour plot of the mode amplitude as a function of the mode frequency and time for slowing down case. The slowing down rate is $\nu=2.0\times10^{-3}\omega_A$.

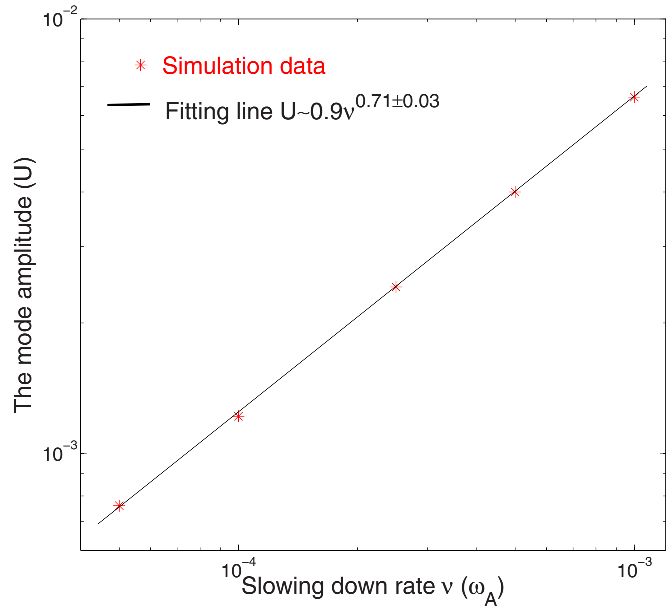

FIG. 9. (Color online) The nonlinear saturation level of the mode amplitude as a function of collision rate in the presence of both pitch angle scattering and slowing down.

nonlinear saturation. However, the saturation level is substantially enhanced at the same value of slowing down rate. From the fitted scaling we can see that the coefficient is about 3.0 times larger but the scaling index is similar as compared to that of the pure scattering case. The enhancement in the saturation level can be explained analytically. First, the pitch angle scattering rate is relatively smaller than the slowing down rate according to the formula $\nu_d=\nu v_c^3/2[(0.17v_0)^3+v^3]$. For the parameters used, the scattering rate is only about one-tenth of the slowing down rate for the resonant particles. Second, because of slowing down is causal rather than stochastic, the particle adiabaticity[14] is maintained so that the trapped resonant particles can stay in resonance with the waves by moving out radially as they slow down. The net effect is that the nonlinear drive is enhanced. Figure 6 shows the resonant region in the phase space without collisions (right) and the resonant region in the presence of slowing down process (left). From this plot, we can see that the resonant region is extended toward plasma edge and lower energy as compared to the collisionless case. This result is consistent with the theoretical prediction.

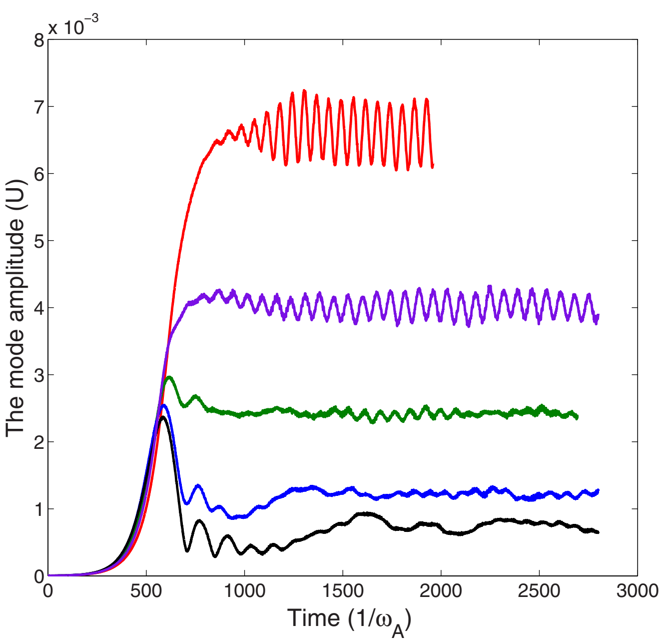

FIG. 8. (Color online) The time evolution of the mode amplitude with both pitch angle scattering and slowing down at different collision rates. From top to bottom, the slowing down rates are $\nu=1.0\times10^{-3}\omega_A$, $\nu=5.0\times10^{-4}\omega_A$, $\nu=2.5\times10^{-4}\omega_A$, $\nu=1.0\times10^{-4}\omega_A$, and $\nu=5.0\times10^{-5}\omega_A$.

Finally, we should note that in these cases of nonlinear evolution with either pitch angle scattering or slowing down, neither the mode structure nor the mode frequency of the TAE changes. Figure 7 shows that the mode frequency is almost fixed during the steady state phase.

It should be pointed out that the explosive behavior will be expected for the near-threshold nonlinear regime when the drag effect dominates over the diffusion in phase space.[34] However, the parameters applied here give a large drive and lead to a strong instability so steady state instead of explosive behavior is obtained. Another important reminder is that the dominance of slowing down effect is only valid for large slowing down regime. When collision (both slowing down and scattering) is weak, the slowing down effect becomes much less significant.

C. Effect of both scattering and slowing down on mode saturation

Finally we perform simulations with both pitch angle scattering and slowing down process. Following the procedure shown above, we have conducted parameter scan for the baseline case. Figure 8 shows the time evolution of mode amplitude for different slowing down rates. Similar to the

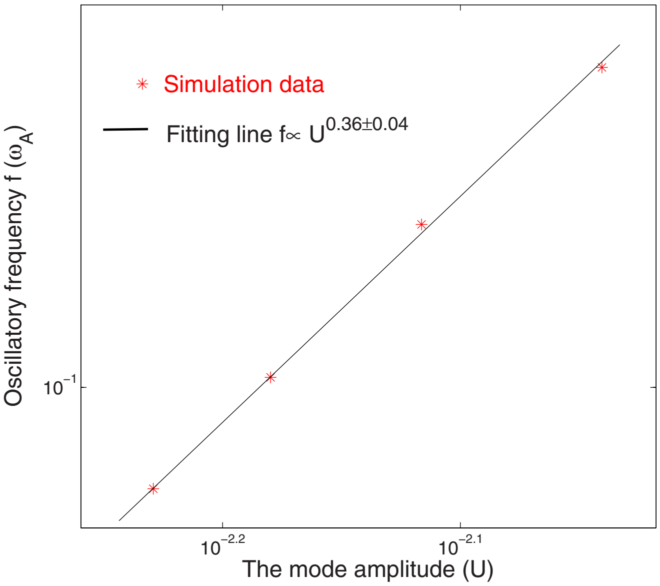

FIG. 10. (Color online) The fast oscillation frequency versus the nonlinear saturation level of the mode amplitude.

cases shown above, the saturation level monotonically increases with the drag rate. For same diffusion and drag rate, the saturation levels in the combined cases are higher than those with only pitch angle scattering or only slowing down. This implies that the enhancement of the saturation level with scattering and slowing down are additive, at least for the range of slowing down rate studied.

Furthermore, Fig. 9 exhibits the scaling between the saturation level and the slowing down rate in logarithmic scale. The linear regression power fit gives the scaling rate as

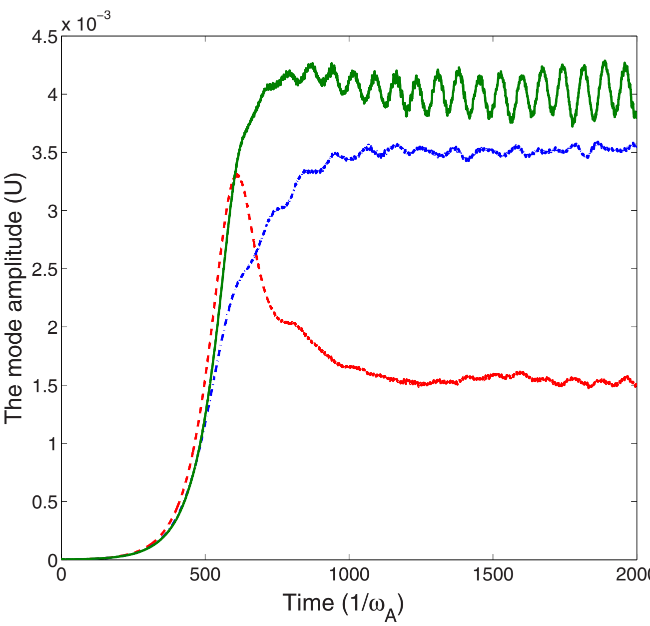

FIG. 11. (Color online) The time evolution of the mode amplitude for different parameter regimes at $\nu=5.0\times10^{-4}\omega_A$. From top to bottom, the first line is for the case with the combination of both slowing down and pitch angle scattering, the second line is for the case with slowing down, and the third line is for the case with pitch angle scattering.

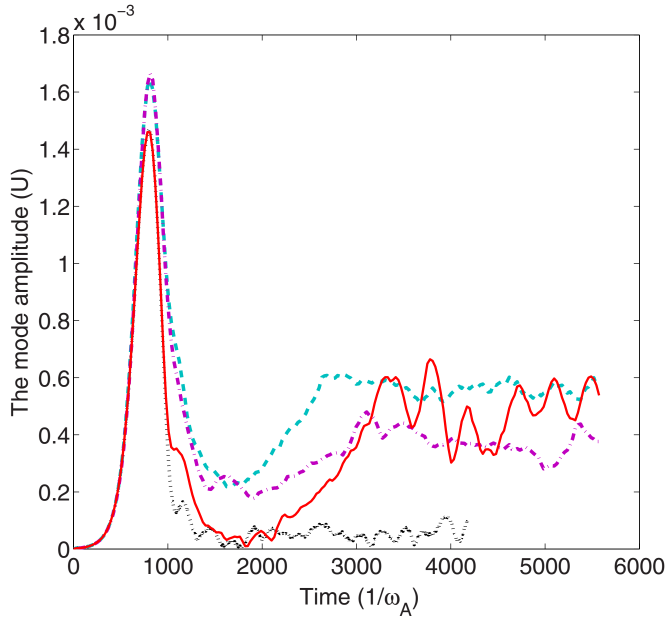

FIG. 12. (Color online) The time evolution of the mode amplitude for different parameter regimes at $\nu=1.0\times10^{-5}\omega_A$. The dotted line is for collisionless case, the dashed line is for the case with the combination of both slowing down and pitch angle scattering, the solid line is for the case with slowing down, and the dashed-dotted line is for the case with pitch angle scattering.

$U\sim0.9\nu^{0.71\pm0.03}$. Compared to the case with only slowing down, we can see that the power index is similar but the coefficient increases by 40%. Again, fast oscillations are observed in this case.

To verify the oscillations shown above are related to trapped particle bouncing motion, we study the scaling between the oscillatory frequencies as a function of the saturation amplitude. Combining the data from pitch angle scattering and slowing cases, we obtain the scaling of oscillatory frequency f versus the saturation amplitude U, as shown in Fig. 10. From this plot we can see that the frequency scales with the amplitude by $f\propto U^{0.36\pm0.04}$. Compared to the theoretical scaling of trapped particle bouncing frequency with the mode saturation amplitude $\omega_b\propto U^{0.5}$, this number is fairly close.

So far we have used relatively large values of slowing down rates (i.e., $\nu>10^{-4}$) as compared to the realistic values of present day tokamak experiments and future burning plasmas. For these large values of slowing down rate, the effects of slowing down are much larger than that of pitch angle scattering in terms of mode saturation level (see Fig. 11), where the slowing down rate is $\nu/\omega_A=5.0\times10^{-4}$. However, analytic theory shows that at sufficiently small slowing down rate, the diffusive process can dominate the nonlinear saturation.[14] Therefore, we now examine a new case of n=1 TAE with a much lower slowing down rate. In this new case, the net linear growth rate and the damping rate are $\gamma/\omega_A=0.9\%$ and $\gamma_d/\omega_A=0.25\%$. The slowing down rate is $\nu/\omega_A=10^{-5}$, which is comparable to the typical values in present day tokamak experiments. Figure 12 shows the time evolution of the mode amplitude for four different cases: no collisions, only pitch angle scattering, only slowing down,

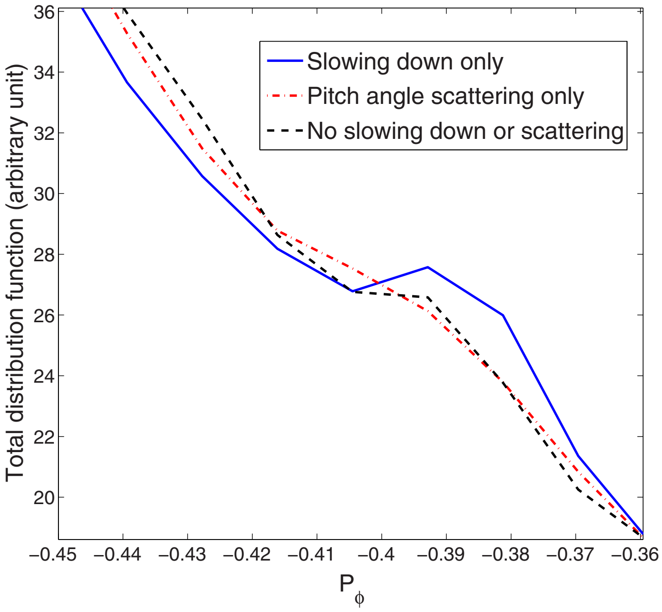

FIG. 13. (Color online) The distribution function as a function of toroidal angular momentum P_ϕ for fixed E and Λ with three cases, collisionless, pitch angle scattering only, slowing down only. The slowing down rate $\nu=5.0\times10^{-4}\omega_A$.

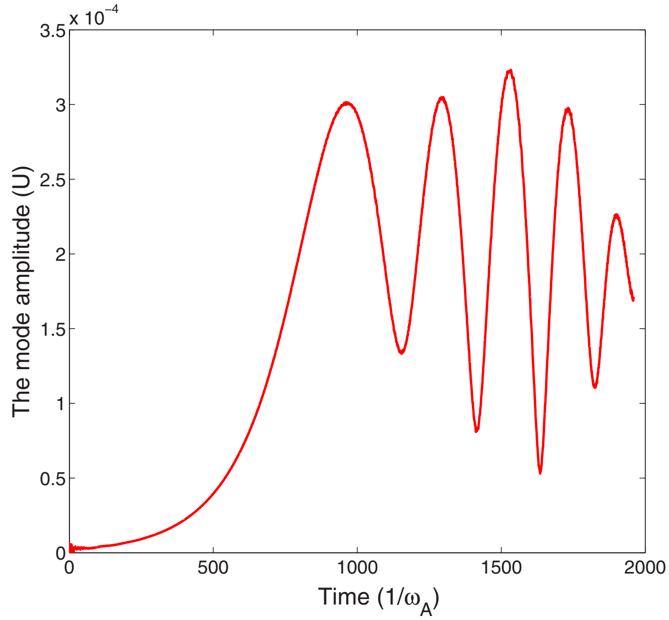

FIG. 14. (Color online) The time evolution of the mode amplitude for the near-marginal instability case. No collisions are present in this case.

and the combination of pitch angle scattering and slowing down. From this plot, we can see that in the initial stage (before $\omega_A t=2000$) the pitch angle scattering effect is dominant and the slowing down process plays little role in affecting the nonlinear saturation level. As time evolves, more particles are slowed down and we can see that slowing down process becomes more important until a nearly steady state is established. In this case, pitch angle scattering and slowing down process are both important for the nonlinear saturation.

D. Particle distribution evolution during nonlinear saturation

As discussed in Secs. III A–III C, the saturation process is different between collisional and collisionless cases. For the collisional cases, the effects of slowing down are different from that of pitch angle scattering. When there are no pitch angle scattering or slowing down, the flattening in the radial profile is the key for nonlinear saturation. The flattening effect quenches the energetic particle drive and this leads the TAE mode to decay to zero due to finite background damping. In the presence of only pitch angle scattering, the diffusive effect tends to restore the radial profile gradient, which competes with the effect of profile flattening. In this way, the effects of pitch angle scattering sustain the mode at a steady level instead of dissipating the mode to zero. For the case of slowing down without pitch angle scattering, the resonant particles can stay in resonance with the wave for a while as they slow down before leaving the resonance. This process also leads to a steady state.[14]

To elucidate the physics involved in the nonlinear saturation of a single TAE mode, we now investigate the evolution of the energetic particle distribution function in detail. We study three different cases, one includes neither the scattering nor the slowing down, one includes the scattering only, and the other one includes slowing down only. Figure 13 shows the energetic particle distribution function versus toroidal angular momentum P_ϕ, where $P_\phi=e\psi+Mv_\parallel RB_\phi/B$ is approximately a radial flux variable. The solid line is for the case with no slowing down or scattering, the dashed line is for the case of pitch angle scattering only, and the dashed-dotted line is for the case of slowing down only. The result is obtained at the same $\Lambda=\mu B/E=0.25$ and the same energy E for all the three lines, but we can clearly see the difference in

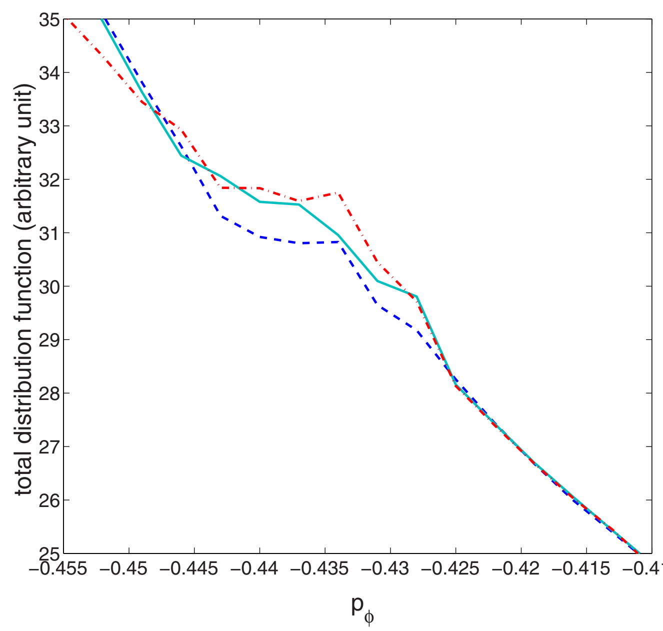

FIG. 15. (Color online) The distribution function as a function of toroidal angular momentum P_ϕ for fixed E and Λ with near-marginal instability at three times, the dashed line corresponds to the first nonlinear drop at $\omega_A t\simeq1060$, the solid line corresponds to the first nonlinear rise at $\omega_A t\simeq1200$, and the dashed-dotted line corresponds to the second nonlinear drop at $\omega_A t\simeq1350$.

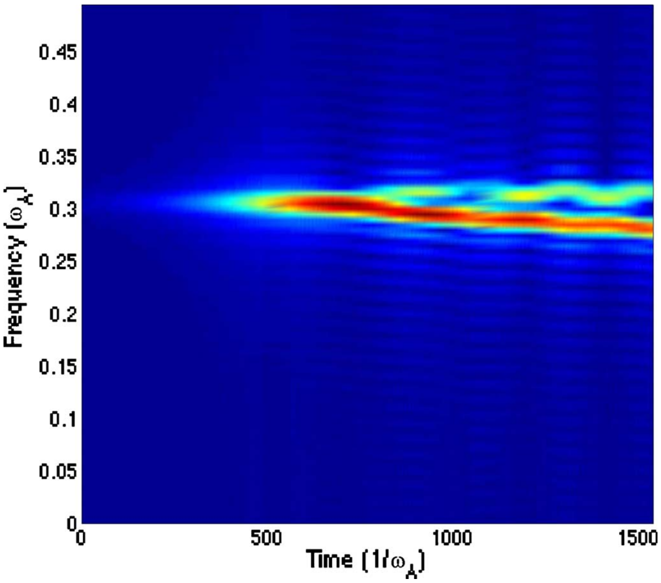

FIG. 16. (Color online) The contour plot of the mode amplitude as a function of the mode frequency and time for near-marginal instability case. No collisions are present in this case.

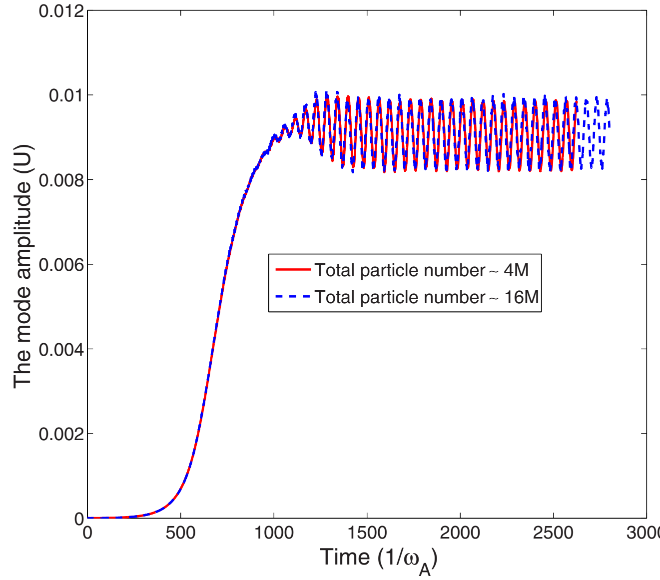

FIG. 17. (Color online) The time evolution of the mode amplitude for different numbers of particles with slowing down only ($\nu = 2.0 \times 10^{-3}\omega_A$), the total number particles used in the dashed line is four times larger than that used in the solid line.

the profile shape as a function of radial position with different parameter regimes. For the case with no diffusion or slowing down, pure flattening effect is observed in the profile during mode decay phase. For the case with only pitch angle scattering, the scattering effect tends to restore the distribution profile and sustain a finite, saturated mode amplitude. From Fig. 13 we can see that a finite slope in the profile is obtained due to scattering instead of pure flattening in the collisionless case. The finite slope retains a nonlinear drive that balances the background dissipation and results in a steady state saturation. The most interesting profile feature corresponds to the case with slowing down only, where a hole-clump-like shape is obtained (dashed-dotted line). It should be noted that there is no frequency shift (as shown in Fig. 7) in the nonlinear regime, which is different from the condition of near-marginal instabilities predicted by theory.[17]

E. Nonlinear saturation of near-marginal instabilities

In the above, we have systematically studied the effects of pitch angle scattering, source, sink, and slowing down based on large drives ($\gamma_L \gg \gamma_d$). If we reduce the drive and increase the background dissipation to the near-marginal instability regime ($\gamma_L \sim \gamma_d$ and $\gamma_L - \gamma_d \ll \gamma_L$), completely different nonlinear behavior is expected according to analytical theory.[17] Here, in our simulations we reduce the drive to ensure the net growth rate comparable to the damping rate, i.e., linear drive $\gamma_L \sim 1.4\%\omega_A$, background damping $\gamma_d \sim 0.8\%\omega_A$, and the new growth rate $\gamma \sim 0.6\%\omega_A$. Figure 14 shows the time evolution of the mode amplitude without collisions. We run weak collision rate $\nu = 5.0 \times 10^{-6}\omega_A$ simulations as well as collisionless simulations. Both cases exhibit similar oscillatory behavior, as shown in Fig. 14, and the oscillatory frequency is independent of the collision rate. This suggests that collisions are not responsible to this nonlinear dynamics and these oscillations could come from the same kind of particle bouncing motion as shown above.

For this case, the nonlinear evolution of the particle distribution is also investigated. Figure 15 shows the shape of the distribution function at resonance as a function of P_ϕ for fixed $\Lambda = \mu B/E$ and E. We find that as the mode amplitude drops, the profile is flattened and as the mode amplitude increases, the profile gradient is restored. The correlation between the oscillatory mode amplitude and the radial profile is consistent with previous observation. However, this kind

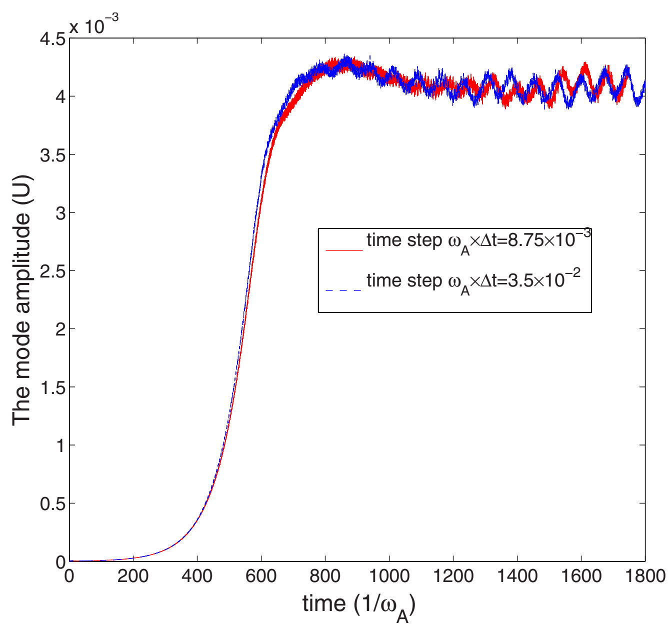

FIG. 18. (Color online) The time evolution of the mode amplitude for different time steps with both pitch angle scattering and slowing down ($\nu = 5.0 \times 10^{-4}\omega_A$), the time step used in the solid curve is 1/4 of that used in the dashed curve.

of profile gradient restoration is not from particle diffusion or particle drag but from the bouncing motion of trapped resonant particles. Figure 16 shows the time evolution of the mode frequency. After the initial nonlinear saturation, the mode frequency slowly chirps up and down. This result is similar to the previous result of Berk *et al.*[18]

IV. CONVERGENCE STUDIES

To confirm the simulation results, extensive numerical convergences have been carried out with regard to the number of particles and the time step. For at least one parameter for each case, we carry out simulations with four times of the particle number or one-fourth of the time step individually. They reproduce the same behavior and similar saturation level. Figures 17 and 18 show the example of our convergence studies in particle number and time step, respectively. Figure 17 is for the case including only slowing down and Fig. 18 is for the case with both pitch angle scattering and slowing down. The slowing down rate used in Fig. 17 is $\nu=2.0\times10^{-3}\omega_A$ and used in Fig. 18 is $\nu=5.0\times10^{-4}\omega_A$. The fast oscillations and the nonlinear saturation level are independent of the time step and the particle number. Therefore, we conclude that we have a good numerical convergence, i.e., the particle number used is sufficient and the time step used is small enough for results presented above.

V. SUMMARY

In summary, kinetic/MHD hybrid simulations are carried out to investigate the nonlinear dynamics of energetic particle-driven toroidal Alfvén eigenmode with collision and source/sink. For cases well above marginal stability, the mode saturation is approximately steady state with finite collision frequency. The simulated scaling of saturation level with collision frequency at three different parameter regimes is studied. For strong pitch angle scattering regime, the saturation level scales with the collision rate by $U\sim0.21\nu^{0.65\pm0.13}$, for weak pitch angle scattering regime, the saturation level scales with the collision rate by $U\sim0.63\nu^{0.68\pm0.06}$, and for moderate pitch angle scattering regime, the saturation level scales with the collision rate by $U\sim0.90\nu^{0.71\pm0.03}$. These scalings agree well with analytic theory. For cases near-marginal stability at low collision rates, the mode saturation exhibits pulsation behavior with frequency chirping up and down. The pulsation is associated with a dynamic relaxation of the particle distribution function in phase space, possibly due to the bounce motion of resonant particles trapped in the waves. Compared to previous work using reduced models, this simulation is unique in its inclusion of both pitch angle scattering and slowing down (with source/sink) in its description of spontaneous nonlinear wave evolution arising from a nonperturbative, fully kinetic/MHD set of equations. In the future, the nonlinear dynamics with multiple modes will be explored.

ACKNOWLEDGMENTS

We gratefully thank H. L. Berk, B. N. Breizman, S. E. Parker, and N. N. Gorelenkov for stimulating discussions. We also thank H. L. Berk and B. N. Breizman for carefully reading the manuscript and for many helpful comments. One of the authors (J.L.) sincerely thanks J. A. Breslau for help in the M3D code diagnostics. This work was supported by the Department of Energy Scientific Discovery through the U.S. Department of Energy under Grant No. DE-AC02-09-CH11466. All simulations are performed on Franklin at the National Energy Research Scientific Computing Center (NERSC).

[1] R. Aymar, V. A. Chuyanov, M. Huguet, Y. Shimomura, ITER Joint Central Team, and ITER Home Teams, Nucl. Fusion **41**, 1301 (2001).
[2] C. Z. Cheng and M. S. Chance, Phys. Fluids **29**, 3695 (1986).
[3] G. Y. Fu and J. W. Van Dam, Phys. Fluids B **1**, 1949 (1989); G. Y. Fu, Ph.D. thesis, University of Texas, 1988.
[4] L. Chen, in *Theory of Fusion Plasmas*, Proceedings of the Joint Varenna-Lausanne International Workshop, Chexbres, Switzerland, 7 October 1988, edited by J. Vaclavik, F. Troyon, and E. Sindoni (Societa Italiana di Fisica by Editrice Compositori, Bologna, 1988), p. 327.
[5] W. Park, E. V. Belova, G. Y. Fu, X. Z. Tang, H. R. Strauss, and L. E. Sugiyama, Phys. Plasmas **6**, 1796 (1999).
[6] L. E. Sugiyama, W. Park, H. R. Strauss, S. R. Hudson, D. Stutman, and X.-Z. Tang, Nucl. Fusion **41**, 739 (2001).
[7] J. A. Breslau, S. C. Jardin, and W. Park, Phys. Plasmas **10**, 1665 (2003).
[8] H. R. Strauss, L. E. Sugiyama, G. Y. Fu, W. Park, and J. Breslau, Nucl. Fusion **44**, 1008 (2004).
[9] G. Y. Fu, W. Park, H. R. Strauss, J. Breslau, J. Chen, S. Jardin, and L. E. Sugiyama, Phys. Plasmas **13**, 052517 (2006).
[10] J. A. Breslau, S. C. Jardin, and W. Park, Phys. Plasmas **14**, 056105 (2007).
[11] J. A. Breslau, C. R. Sovinec, and S. C. Jardin, Comm. Comp. Phys. **4**, 647 (2008).
[12] R. Paccagnella, H. R. Strauss, and J. Breslau, Nucl. Fusion **49**, 035003 (2009).
[13] H. L. Berk and B. N. Breizman, Phys. Fluids B **2**, 2226 (1990).
[14] H. L. Berk and B. N. Breizman, Phys. Fluids B **2**, 2235 (1990).
[15] H. L. Berk and B. N. Breizman, Phys. Fluids B **2**, 2246 (1990).
[16] H. L. Berk, B. N. Breizman, and H. Ye, Phys. Rev. Lett. **68**, 3563 (1992).
[17] B. N. Breizman, H. L. Berk, M. S. Pekker, F. Porcelli, G. V. Stupakov, and K. L. Wong, Phys. Plasmas **4**, 1559 (1997).
[18] H. L. Berk, B. N. Breizman, J. Candy, M. Pekker, and N. V. Petviashvili, Phys. Plasmas **6**, 3102 (1999).
[19] G. Y. Fu and W. Park, Phys. Rev. Lett. **74**, 1594 (1995).
[20] S. Briguglio, G. Vlad, F. Zonca, and C. Kar, Phys. Plasmas **2**, 3711 (1995).
[21] Y. Todo and T. Sato, Phys. Plasmas **5**, 1321 (1998).
[22] Y. Todo, K. Shinohara, M. Takechi, and M. Ishikawa, Phys. Plasmas **12**, 012503 (2005).
[23] S. Briguglio, G. Fogaccia, G. Vlad, F. Zonca, K. Shinohara, M. Ishikawa, and M. Takechi, Phys. Plasmas **14**, 055904 (2007).
[24] Y. Nishimura, Phys. Plasmas **16**, 030702 (2009).
[25] A. Mishchenko, A. Knies, and R. Hatzky, Phys. Plasmas **16**, 082105 (2009).
[26] J. Lang, Y. Chen, S. E. Parker, and G. Y. Fu, Phys. Plasmas **16**, 102101 (2009).
[27] H. L. Berk, B. N. Breizman, and M. S. Pekker, Nucl. Fusion **35**, 1713 (1995).
[28] H. V. Wong and H. L. Berk, Phys. Plasmas **5**, 2781 (1998).
[29] J. Candy, H. L. Berk, B. N. Breizman, and F. Porcelli, Phys. Plasmas **6**, 1822 (1999).
[30] Y. Chen, R. B. White, F. Guo-yong, and R. Nazikian, Phys. Plasmas **6**, 226 (1999).
[31] Y. Todo, H. L. Berk, and B. N. Breizman, Phys. Plasmas **10**, 2888 (2003).
[32] Y. Todo, T.-H. Watanabe, H.-B. Park, and T. Sato, Nucl. Fusion **41**, 1153 (2001).
[33] A. H. Boozer and G. Kuo-Petravic, Phys. Fluids **24**, 851 (1981).
[34] M. K. Lilley, B. N. Breizman, and S. E. Sharapov, Phys. Rev. Lett. **102**, 195003 (2009).